International Journal of Engineering and Geosciences
https://dergipark.org.tr/en/pub/ijeg
e-ISSN 2548-0960

A new approach to soil moisture estimation based on correlation between SAR and multispectral indices and seasonal pattern of soil moisture dynamics: a case study of Lake Urmia Basin

Maryam Sadeghi [1], Khalil Valizadeh Kamran*[2], Sadra Karimzadeh[3], Abolfazl Ghanbari[4], Saeed Samadianfard[5]

[1]*Department of Remote Sensing and GIS, University of Tabriz, Tabriz, Iran. Sadeghi.maryam@tabrizu.ac.ir[2], Department of Remote Sensing and GIS, University of Tabriz, Tabriz, Iran. valizadeh@tabrizu.ac.ir, [3]Department of Remote Sensing and GIS, University of Tabriz, Tabriz, Iran. sadra.karimzadeh@gmail.com,[4]Department of Remote Sensing and GIS, University of Tabriz, Tabriz, Iran. a_ghanbari@tabrizu.ac.ir,[5]Department of Water Engineering, Faculty of Agriculture, University of Tabriz, Tabriz, Iran. samadianfard@gmail.com.*

Cite this study: Sadeghi, M., Khalil Valizadeh, Kh., Karimzadeh, S., Ghanbari, A. & Samadianfard, S. (2026). A new approach to soil moisture estimation based on correlation between SAR and multispectral indices and seasonal pattern of soil moisture dynamics: a case study of Lake Urmia Basin. International Journal of Engineering and Geosciences, 11(2), 392-407.

https://doi.org/10.26833/ijeg.1734366

Keywords
Soil Moisture
SAR Indices
Correlation Analysis
Machine Learning
lake Urmia basin

Research/Review Article

Received:08.07.2025
1.Revised: 06.09.2025
2.Revised: 28.09.2025
Accepted:28.09.2025
Published:01.07.2026

Abstract

Radar satellite imagery has been widely used to obtain soil moisture (SM) estimates of high accuracy. Accurate information on surface soil moisture content under scalable conditions is important for hydrological and climatological applications. the aim of this study, the integration of multi-sensor satellite data to investigate the importance of features in various products and estimate soil moisture, is conducted using two machine learning models, Random Forest (RF) and Support Vector Regression (SVR), in the Lake Urmia basin. we used Sentinel-1 C-band Synthetic Aperture Radar (SAR) data, Sentinel-2 and Landsat-8 optical-thermal imagery, soil property maps (SoilGrids), and climate variables (FLDAS). at first analysis of correlation and regression was done seasonally for the four-year period to examine the importance and effectiveness of their use in estimating soil moisture. Then, the implementation of the model was done in two stages, using all the features (22) and 10 that were determined based on the performance of the model. The results show that soil organic carbon (SOC250) and radar indices governed winter and spring moisture dynamics, whereas vegetation indices dominated summer and autumn predictions, reflecting vegetation-climate-soil interactions. The Rand Forest model using all features had the highest accuracy of 0.88 in spring and the lowest in summer, with an accuracy of 0.80, while the SVR model had the lowest accuracy in summer (50.539) and the highest accuracy (0.628) in autumn, with the SVR results using the 10 most important features increasing by 0.1 R2 across all the variables. This increase in accuracy was observed in the RF model from 0.1 to 0.3, with the highest increase in accuracy in the summer. RF outperforms the SVR model in all evaluation metrics, including Mean Squared Error (MSE), R^2, and Mean Absolute Error (MAE), for both feature sets and in all seasons. The Normalized Vegetation Structural Difference Index (NVSDI) and Normalized Radar Vegetation Difference Index (NRVDI) indices have helped improve model accuracy by providing more combined and detailed information about specific soil and vegetation characteristics. normalized difference vegetation index (NDVI) has a specific focus on vegetation, while NVSDI and NRVDI provide more comprehensive and detailed environmental information. These findings demonstrate the potential of multi-sensor data integration seasonally, for soil moisture estimation, providing and critical insight for hydrological modeling, monitoring environmental and agricultural.

1. Introduction

Soil moisture is an essential component in hydrological and climate systems, and plays an important bridging function between the Earth's surface and the atmosphere. Spatial distribution and temporal variation in soil moisture vary in different areas [1, 2]. Advances in technology have enhanced agricultural yields, where accurate SM estimation plays a vital role in irrigation scheduling, a key issue in agriculture [3]. Traditional SM monitoring methods are labour-intensive

and lack sufficient spatial coverage [4, 5]. SM's high spatiotemporal variability further complicates its measurement. Satellite remote sensing thus offers a powerful alternative for large-scale SM estimation [6]. This study aims to develop a scalable, high-resolution soil moisture estimation framework for various seasons by integrating SAR and multispectral indices, tailored for complex landscapes such as the Lake Urmia Basin. Several approaches combining optical and microwave remote sensing data have been proposed for SM [7].

Remote sensing techniques encompass optical, thermal [8], and microwave (both active and passive) domains [9, 10], generating valuable global datasets [11], and climate products [12]. For instance, a hybrid methodology using Sentinel-1, Sentinel-2 [13], and in-situ data from the International Soil Moisture Network (ISMN) has been tested across different climatic contexts [14] [15]. Similarly, the SMOS and SMAP missions utilize passive microwave observations to support hydrological and climate research [16, 17]. In a complementary approach, AirSAR and Landsat sensors have been employed under varied soil moisture conditions and vegetation levels, demonstrating the utility of both optical and radar data for vegetation monitoring [18].

Despite advancements, accurate measurement remains challenging in heterogeneous areas [19]. Optical methods face cloud cover limitations [20], while microwave sensing, though all-weather capable and sensitive to soil moisture [16, 21], is affected by vegetation interference [22]. Integration of multispectral and SAR data addresses this [16, 23, 24], using optical indices (e.g., LAI, VCI, VHI, TCI, LST) from Sentinel-2/Landsat to quantify vegetation impacts [13, 25–27], alongside radar-specific indices (e.g., RVI, DPDD, DPSVI, VDDPI) adapted for Sentinel-1 [27–29]. This combined approach significantly improves accuracy by correcting vegetation-induced errors in radar signals [13, 15, 16, 30, 31].

Among various remote sensing techniques, Synthetic Aperture Radar (SAR) has demonstrated significant potential for high-resolution soil moisture estimation at the watershed and field scale [3, 7, 28, 29, 32].

This capability has been further enhanced by machine learning (ML), which has emerged as a powerful tool for understanding and predicting soil behavior [39,41]. ML's ability to handle complex, non-linear relationships and multivariable factors has driven its adoption in soil moisture prediction [33]. with expanding applications in satellite-based monitoring and downscaling [34]. While model performance varies across environmental settings and depends on data quality and quantity [35], ML excels at processing large-scale complex datasets to extract intricate patterns often missed by conventional methods [35]. Common ML algorithms for soil moisture estimation include Support Vector Regression (SVR), [36, 37] Artificial Neural Networks (ANN) [38, 39]Random Forest(RF) [36], and eXtreme Gradient Boosting (XGBoost)[40]. Among these, RF has been widely used for spatial variable prediction [37], while SVM/SVR approaches have been extensively applied across various domains [41]. Empirical comparisons frequently show superior performance of RF and SVM/SVR over other methods, with RF often achieving the highest accuracy in classification tasks [30, 42]. A consensus confirms that both RF and SVR models are highly efficient for estimating soil moisture levels [20, 43–45].

This study focuses on soil moisture prediction in the Lake Urmia basin, a major global climate hotspot where hydrological studies remain limited due to data scarcity. Soil moisture measurement here is particularly challenging due to high spatial variability in soil depth, relief, soil type, vegetation cover, and land use. Additionally, environmental factors such as temperature, rainfall, and evapotranspiration further complicate accurate measurements [46]. To address these challenges, this study is the first to integrate the effectiveness of a scalable multi-sensor framework with an emphasis on Sentinel-1 imagery, combined with a comprehensive dataset (Sentinel-2 and Landsat-8 optical-thermal imagery, SoilGrids, and FLDAS) in the Urmia Lake basin. Soil moisture estimation for the period 2020-2024 was performed using two machine learning models (RF and SVR), considering seasonal prioritization of features. Also, the moisture stress indices LST, VHI, and VCI were evaluated for seasonal moisture estimation. Among them, LST was of great importance, especially in summer. It is worth noting that two composite, multispectral, and radar indices, NRDVI and NVDSI, were proposed in this study, which complement the vegetation survey with higher efficiency than single indices and can be useful in moisture stress monitoring.

2. Materials and methods

2.1. Study Area

The Lake Urmia basin spans approximately 52,000 km^2 in northwest Iran [47]. situated between latitudes 36°26' to 38°16' N and longitudes 45°2'5" to 46°15' E, covering parts of the western and eastern Azerbaijan and Kurdistan provinces (Figure 2) [48]. Lake Urmia is one of the largest permanent hypersaline lakes on Earth, serving as a critical habitat for diverse bird species, contributing to its global ecological importance. The basin supports about 7.9 million people, with key urban centers such as Tabriz, Maragheh, and Bonab. The surrounding regions are fertile agricultural lands, heavily dependent on water resources. The local economy integrates both agricultural and industrial activities, both of which rely significantly on the lake's hydrological systems [46]. In recent years, 35 dams have been constructed across 21 rivers feeding into Lake Urmia to facilitate agricultural development in the region. Nonetheless, due to decreased surface water and increased salinity, the lake has been in a precarious state in recent years [47]. Lake Urmia has experienced significant shrinkage due to natural and anthropogenic factors, including decreases in air fronts originating from Europe and cold regions [48]. Agriculture in the Lake Urmia basin is highly reliant on precipitation and increased temperatures attributed iant on river irrigation canals, which have led Lake Urmia water levels to fall in recent years [49]. Dams have increased demand for industrial and household purposes, causing a long-term drought in the area and a reduction in Lake Urmia's water[46].

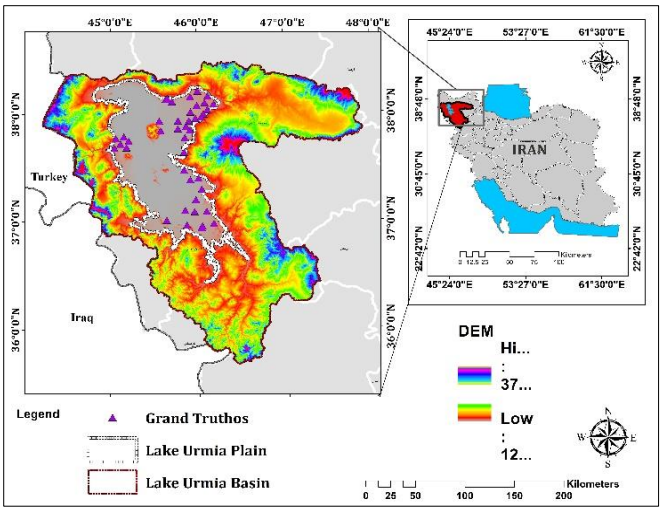

Figure 1. The study area location and Grand Truths

2.2. Data Description

The study used SoilGrids data (https://soilgrids.org/) at 1,000-meter and 250-meter resolutions, along with FLDAS weather data, including precipitation and evaporation, to evaluate soil moisture trends at a depth of 5 cm. SoilGrids is a global soil mapping platform developed by the International Soil Reference and Information Center (ISRIC) [50, 51], which uses machine learning algorithms and environmental data to generate high-resolution maps of soil properties. In an innovative step to investigate the relationship between parameters extracted from radar and multispectral images and their effects on seasonal soil moisture fluctuations, we combined spatial soil characteristics from SoilGrids with weather-driven soil moisture estimates from FLDAS to create the Soil Moisture Fusion Dataset (SMFD). This integrated dataset provides a comprehensive representation of soil moisture dynamics, capturing seasonal patterns and regional variations. SMFD offers a solid foundation for analyzing soil moisture behavior at different spatial and temporal scales.

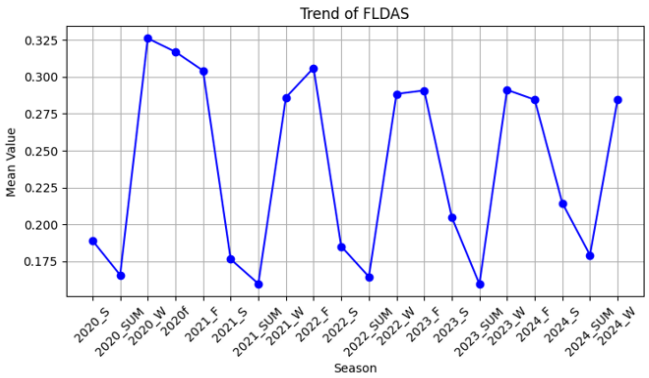

[1] SoilGridsV2 provides global gridded soil property maps derived from ML-based aggregation of thousands of soil profiles and environmental covariates

Figure 2. Seasonal trends in surface soil moisture based

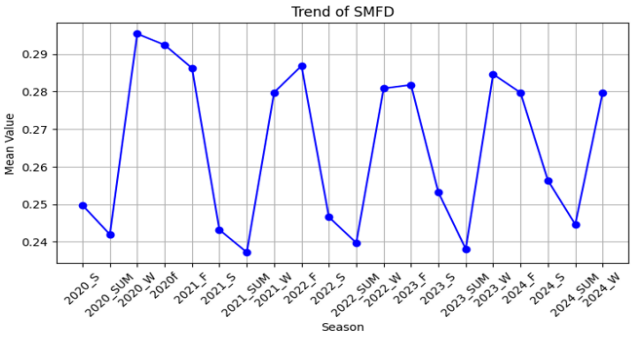

on data from the Famine Early Warning Systems Network Land Data Assimilation System (FLDAS) and soil moisture fusion dataset (SMFD).

Sentinel-1 Level-1 GRD IW swath images with VV and VH polarizations [14] in descending mode, a total of 147 images were employed for radar-based moisture estimation. These images, processed to 10 × 10 m Ground Range Detected (GRD) products, were derived from raw Single-Look Complex (SLC) data (5 × 20 m resolution) through multi-looking, geocoding, and subswath stitching [52, 53]. Additionally, 598 Sentinel-2 Level-2 images (mosaics of four images per entry), covering 10 spectral bands in Visible (VIS), Near-InfraRed (NIR), and ShortWave InfraRed (SWIR) with spatial resolutions of 10, 20, and 60 m, were acquired. Sentinel-2 images were acquired with a time lag of less than 5 days relative to Sentinel-1, balancing data availability. This time lag introduces uncertainties due to the dynamic nature of Vegetation Water Content (VWC), which can vary substantially over short timescales, influenced [36]. Additionally, 105 Landsat-8 images were utilized to derive vegetation information using spectral indices and surface temperature. The datasets used in this study are summarized in Table 1, which includes satellite characteristics, orbital paths, number of images, and ground samples.

Table 1. Data used in this study

Sensor/ Dataset	Orbit Pass / Sensor Type	Number of images	Number of samples
Sentinel-1	Descending/SAR	147	5836
Sentinel2/A, B	Multispectral bands	598	5836
Landsat-8	Multispectral bands and TIR (Thermal Infrared) bands	105	5836
SoilGridsV2 [1](OpenLandM)	Soil property (ML-based, gridded)	-	5836
FLDAS	Climate reanalysis	Seasonal average	5836

A total of 5,836 samples, as mentioned in Table 1, Data from all sources were aggregated to a 100-meter spatial grid and averaged seasonally over 4 years. Data collection, preprocessing, and the calculation of derived

indices (e.g., vegetation and thermal indices from This Sentinel-2, dipole dispersion coefficients from Sentinel-1) were conducted on this seasonally aggregated dataset to prepare inputs for machine learning modeling. approach ensures that both spatial heterogeneity and temporal variability are captured for accurate surface soil moisture estimation. with additional information provided below. The dipole dispersion coefficients of VV and VH acted as initial inputs for radar-based soil moisture recovery ،While the Sentinel-2 surface reflection data provided vegetation parameters through spectral indicators. This dataset evaluates the correlation between these parameters and surface soil moisture, and the performance of the RF model machine learning algorithm, which is commonly used to estimate surface soil. This data set was used to evaluate the performance of the common collision forest model machine learning algorithm to estimate surface soil.

2. 3. Methodology

2. 3.1. SAR Vegetation Indices

The synergistic use of SAR and multispectral data is crucial for comprehensive vegetation and soil moisture

monitoring, as they provide complementary information on structural (e.g., canopy geometry from SAR) and biochemical (e.g., chlorophyll content from multispectral data) vegetation characteristics. This study leveraged Sentinel-1 C-band SAR data, particularly sensitive to soil moisture variations in the VV polarization (Table 2) [54].

To account for the effects of vegetation on backscatter,

Numerous vegetative descriptors have been developed. In this study, fourteen dual-polarization GRD SAR and multispectral-derived vegetation descriptors were utilized. Key indices included SAR-based indices such as RVIdp [61], and the Dual-Polarization SAR Vegetation Index (DPSVI), which distinguishes vegetation from bare soil using Euclidean distances between VV and VH backscatter [66]. Traditional multispectral indices, including NDVI and LAI, were also employed for soil-vegetation-atmosphere modeling [59, 67]. This combination enables comprehensive characterization of vegetation-soil moisture interactions. Seasonal averages of these indices (2020-2024) were calculated from preprocessed imagery and served as critical inputs for machine learning models.

2. 3. 2. Processing in GEE

In this study, Google Earth Engine (GEE) was employed as the primary platform for data integration, preprocessing, and analysis over the period 2020 to 2024. [68]Essential pre-processing steps supported by GEE include thermal noise removal, radiometric calibration, border noise modification, spot filtering, and ground modification using a 30-meter high digital height model, which ensures data compatibility and geometric accuracy for a wide range of applications [58, 69]. All additional preprocessing is optional and can be adjusted by the user depending on specific requirements and application needs. This preprocessing, such as Speckle Filtering, ensured high-quality, geocorrected radar backscatter data for further analysis[70]. Multispectral data from Sentinel-2 and Landsat-8 were also accessed and processed in GEE. The platform facilitated combining these multi-sensor datasets with soil property and climate-driven datasets for comprehensive soil moisture modeling. Additionally, GEE's cloud computing capabilities allowed efficient extraction [19, 71]. The use of GEE enabled scalable, reproducible analysis with timely access to updated satellite data, crucial for this study's integrated soil moisture estimation approach. In this study, in the GEE environment, following preprocessing and spatiotemporal filtering of the images, various spectral indices were calculated. Their seasonal averages were collected in combination with the climatic dataset of soil properties. As a data point dataset in combination with GPS points from the study area was used to increase spatial accuracy. Then prepared in a GIS environment, as the collected dataset was used as critical input features for machine learning models implemented in Google Colab [51, 64]. This combination enables comprehensive characterization of vegetation-soil moisture interactions. Seasonal averages of these indices (2020-2024) were calculated from preprocessed imagery and served as critical inputs for machine learning models.

2.3. 3. Machine Learning Algorithms

The RF and SVR machine learning algorithms were employed to estimate surface soil moisture using combined Sentinel-1 SAR, Sentinel-2 multispectral imagery [72], and the SoilGrid Dataset. The RF algorithm, developed by [32, 73], is an ensemble learning method that combines decision trees and bagging for classification and regression tasks. It builds multiple decision trees using random subsets of features and data, enhancing model robustness and accuracy [36, 74, 75]. This approach improves robustness against overfitting and noise inherent in remote sensing datasets and adapts well to diverse spatiotemporal scales [76]. The SVR algorithm, an extension of the Support Vector Machine (SVM) developed by Vapnik in the 1990s for regression problems, applies SVM principles to regression [36, 47]. SVR is an important application of the SVM to regression problems. Using SVR as a regression analysis needs to find a hyperplane, such as SVM. The difference is that it needs to find a plane in SVM to make the support vectors or all data of two classification sets farthest from the classification plane, while SVR is to find a regression plane to make all data of a set closest to the plane, which is suitable for solving the regression problem in the case of small samples [77]. To select the best parameters, gamma, epsilon, and C were tuned for SVR, while RF parameters such as the number of trees and maximum depth were optimized. This systematic parameter tuning improves model generalization and performance. The RF model was configured with 100 trees (n_estimators=100) and a random_state=45 to ensure reproducibility in data splitting and random sampling. The selection and tuning approach is consistent with scikit-learn documentation and supported by numerous SVR tuning studies, although implementation details vary among studies [89,64]. The method of this

technique systematically evaluates combinations of these parameters to improve the generalization and performance of the model. The RF model with 100 trees (n_estimators=100) and the value of random_state=45 was used to ensure repeatability in the data splitting process and random sampling [53, 79]. In the selection of the machine learning model, as documented in scikit-learn and supported by numerous studies on SVR tuning, it is consistent. Implementation specifics vary across studies.

that 80% of the dataset was used to train the models, while the remaining 20% was reserved for evaluating model accuracy [80]. this selection process enhances model efficiency by reducing dimensionality while preserving predictive. The 22 Features were standardized using StandardScaler before training. The RF model was trained and evaluated using MSE, R^2, and MAE [91]. The RF model was trained and evaluated using MSE, R^2, and MAE [91]. The general procedure followed in this study is illustrated in Figure 3, depicting the flowchart of the overall process.

Index	Formula	Description	Reference
RVI (Radar Vegetation Index)	RVI=$\frac{4.\sigma^{\circ}_{VH}}{\sigma^{\circ}_{VV}+\sigma^{\circ}_{VH}}$	σ^0VH: VH polarization backscatter intensity σ^0VV: polarization backscatter intensity	[55]
PRVI Polarimetric Radar Vegetation Index	PRVI=(1-$m_c)\sigma_{vh}(\frac{2q}{1+q}q_{vh})$	Where, $0 \le q = \sigma vh\frac{\sigma vh}{\sigma vv} \le 1$, q = $\frac{vh_i)}{vv_i}$	[56]
IDPDD (Inverse Dual-Pol Diagonal Distance)	IDPDD=$\frac{vv_{max}-vv_i)+vh_i}{\sqrt{2}}$	σvv(max) is the maximum value observed in VV polarized imagery. σvv(i) is a value of the ith pixel in VV polarized imagery. The minimum diagonal distance of the Soil-Vegetation Edge represents soil or barren land, and as the distance increases, it indicates the presence of vegetation. Hence, the pixels located at the maximum diagonal distance indicate the presence of vegetation.	[57]
DPDD (Dual-Pol Diagonal Distance)	IDPDD= $\frac{(vv_i+(vh_i)}{\sqrt{2}}$	$VV(i)$ and $VH(i)$ are the VV and VH band values, respectively, in the pixel at the coordinate (i). This index has a higher potential to separate the pixels representing vegetation from pixels of bare soil (which also includes settlements and other bare surfaces).	[41, 58]
VDDPI (Vertical Dual de-Polarization Index)	VDDPI=$\frac{vv_i+vh_i)}{vv_i}$	Where $VV(i)$ and $VH(i)$ are the VV and VH band values, respectively, in the pixel at the coordinate (i). The ratio between total polarized power and co-polarized power. This parameter estimates the degree to which the surface depolarizes the transmitted signal under investigation.	[41, 50]
DPSVI (Dual Pol Soil Vegetatio[25]n Index)	DPSVI= ($IDPDD_i$* $VDDPI_i$*σvh_i) IDPDD= $\frac{\sigma 0VV_{max}-\sigma 0VV)+\sigma^{\circ}VH}{\sqrt{2}}.\frac{\sigma^{\circ}VV+}{\sigma^{\circ}V}$	DPSVI is a product of two other indices: IDPDD and VDDPI. The IDPDD distinguishes pixels of water and/or vegetation from bare soil pixels. the index is mathematically normalized, and the resulting value increases with the increased amount of above-ground biomass.	[59, 60]
NDVI (normalized difference vegetation index)	NIR – RED/NIR + RED	utilized higher-resolution Sentinel-2A/B satellite data with 10 m resolution	[53, 61]
LAI (Leaf Area Index)	EVI = 2.5 * $\frac{(NIR-RED)}{(NIR+6*RED-7.5*}$ LAI= 3.618×EVI−0.118	where the bands are selected as: RED: band B4 NIR: band B5 BLUE: band B2	[59]
LST (Land Surface Temperature)	$T_{s=}\frac{k_2}{(Ln\frac{K1}{Ly}+1)}$ − 273.1	BT: brightness temperature (0C) K : thermal constants (W/(m2.sr.μm) and K), found in METADATA file; 273.1: subtracted to return the temperature in Celsius	[62]
VCI 9Vegetation Condition Index)	$(NDVI-NDVI_{min}/NDVI_{max}-NDVI_{min})$	where NDVI is the value for the pixel and month and NDVImin and NDVImax are the minimum and maximum values of NDVI over the whole period of 2020–2024, for the considered pixel and month.	[10]
TCI (Thermal Condition Index)	$(LSTmax-LST/LSTmax+LSTmin)*100$	It should be noticed that Kogan (1997)	[9, 25, 64]
VHI (Vegetation Health Index)	$\alpha VCI + (1-\alpha)\,TCI$	where α is a weight parameter that is usually set as α = 0.5	[65]
NRVDI (Normalized Radar Vegetation Difference Index)	RVI - PRVI / RVI + PRVI	NPVDI leverages SAR data to detect subtle structural and polarimetric variations in vegetation canopies.	-
NVSDI (Normalized Vegetation Structural Difference Index)	DPSVI – LAI / DPSVI + LAI	RADAR Normalized Difference Vegetation Index	-

Table 2. Description of extracted vegetation features

Table 3. Describing and summarizing the characteristics used and the statistical summary

Name	Features	Description	Mean	Std	Min	Max
Features Selected from Sentinel-1	RVI	Radar Vegetation Index	0.84	0.04	0.43	0.94
	IDPDD	Integrated Drought Prediction and Detection Index)	0.45	0.13	0.04	0.89
	VDDPI	Vegetation Drought Performance Index	0.66	0.01	0.48	0.99
	PRVI	Polarimetric Radar Vegetation Index	0.67	0.08	0.32	0.90
	DPSVI	Calculeat from VDDPI and *IDPDD* index	0.64	0.01	0.51	0.90
	Angle	Incidence Angle	0.38	0.19	0.00	1.00
	VV	Vertical-Vertical Polarization	0.50	0.11	0.00	1.00
	DPDD		0.49	0.12	0.00	0.90
	VH	Vertical-Horizontal Polarization	0.48	0.15	0.00	1.00
	SOC	Soil Organic Carbon	0.69	0.20	0.00	1.00
Features Selected from the SoilGrid Dataset	Bulk D250	Bulk Density	0.28	0.14	0.00	1.00
	Sand250	Sand Content 250m	0.72	0.34	0.00	1.00
	PH1000	pH (soilgrids/latest/data_aggregated)	0.36	0.17	0.00	1.00
	Sand1000	Sand (soilgrids/latest/data_aggregated)	0.44	0.19	0.00	1.00
	VCI	Vegetation Condition Index	0.36	0.20	0.00	1.00
Features Selected from Sentinel-2 and Landsat-8 Multispectral Data	TCI	Temperature Condition Index	0.56	0.15	0.00	1.00
	NDVI	Normalized Difference Vegetation Index	0.42	0.09	0.00	0.80
	LAI	Leaf Area Index	0.44	0.12	0.00	0.77
	LST	Land Surface Temperature	0.40	0.18	0.00	1.00
	VHI	Vegetation Health Index	0.56	0.15	0.00	1.00
	DNDVI	RADAR Normalized Difference Vegetation Index	0.78	0.01	0.00	1.00
Selected Features Composed of SAR and Multispectral Data	NRVDI	Normalized Radar Vegetation Difference Index	0.18	0.17	0.04	0.96
	SMFD	combines spatial soil property information from SoilGrids (at 1000 m and 250 m resolutions) with climate-driven soil moisture estimates from FLDA	0.28	0.12	0.10	0.75
Climate-Driven Soil Moisture	FLDAS	Famine Early Warning System Land Data Assimilation System	0.24	0.08	0.14	0.41

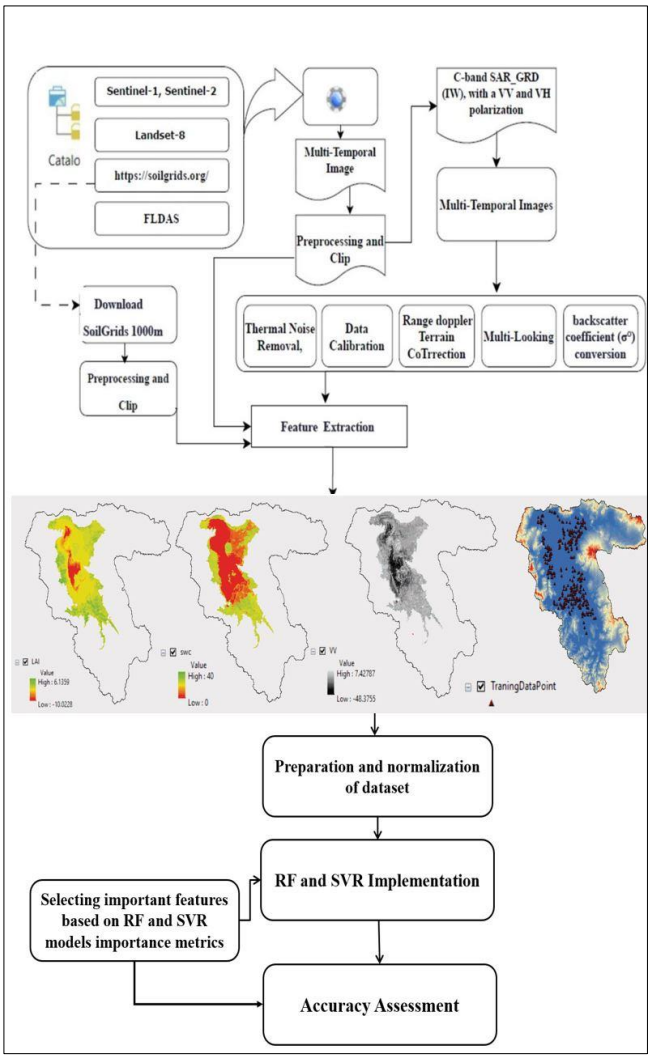

Figure 3. Workflow for soil moisture estimation

4. Results and Discussion

4.1. Analysis of the Relationship Between Features and Soil Moisture

Seasonal variations affect the correlations between key environmental variables and the SMFD. These variations highlight the complex interactions influencing soil moisture dynamics in spring. The correlation matrix (Figure 4) analyzes the relationships between various parameters and seasonal humidity. The findings reveal strong positive correlations among radar-based indicators; for example, VV and DPDD (R = 0.93), and VV and VH (R = 0.81). Moreover, DPDD is highly correlated with PRVI (R=0.96). DPSVI exhibits nearly perfect negative correlations with LAI and NDVI (R=-0.9 each), indicating suppressed canopy development. Soil texture variables show modest correlations (0.4) with vegetation indices, while thermal variables such as LST display weak negative correlations with NDVI (R = -0.20) and SMFD (R = -0.24). TCI and VCI are moderately negatively correlated (R = -0.36). Vegetation structural indices, NRVDI, are clearly characterized by high correlation values. Overall, vegetation indices LAI and NDVI demonstrate robust, seasonally consistent positive correlations with SMFD, particularly during summer and

winter. Radar variables VV and VH show stable moderate correlations (R = 0.3–0.4), whereas soil and thermal factors exert weaker, season-dependent influences. These seasonal variations underscore the dynamic complexity of soil moisture regulation, emphasizing the critical need to consider both temporal and environmental factors when selecting key predictors to enhance the accuracy of ecological and hydrological models.

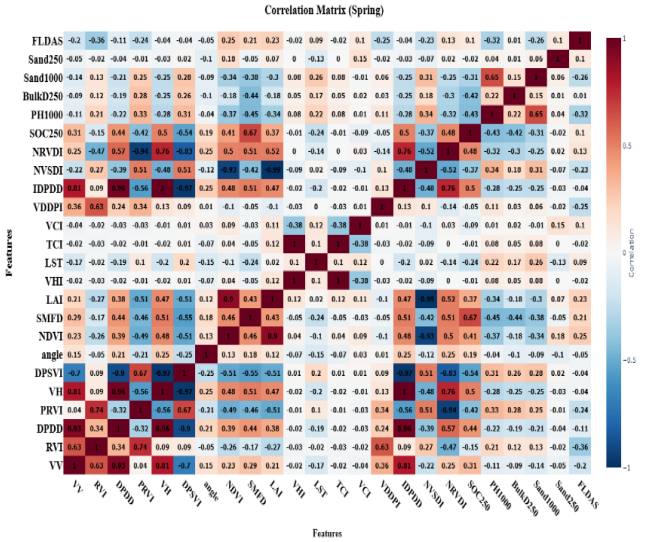

Figure 4. Correlation matrices coefficients between various independent variables and the Soil moisture fusion dataset (SMFD) in the spring.

Soil Moisture Correlation Analysis Across Seasons

The bar charts present the correlation between the feature and SMFD during four distinct seasons (Figure 5). Radar indices such as VV, RVI, DPDD, and VH show moderate to strong positive correlations (approximately 0.3 to 0.65) with SMFD. Conversely, soil texture parameters, including sand content, demonstrate negative correlations, reflecting reduced moisture retention in sandy soils. Vegetation indices such as LAI and NDVI show positive correlations in the spring and winter. These seasonal analyses highlight the complex, dynamic relationships between soil moisture and environmental factors, emphasizing the importance of integrating multi-sensor data to accurately capture soil moisture variability throughout the year.

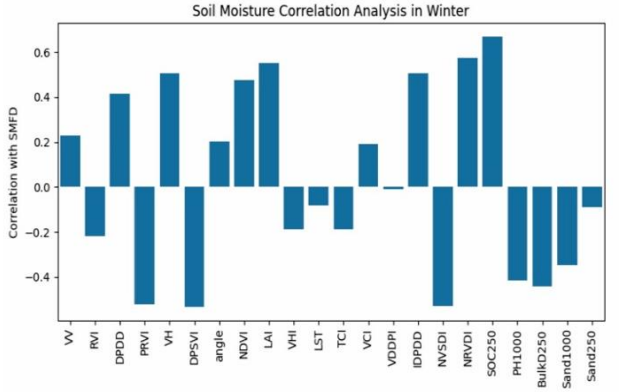

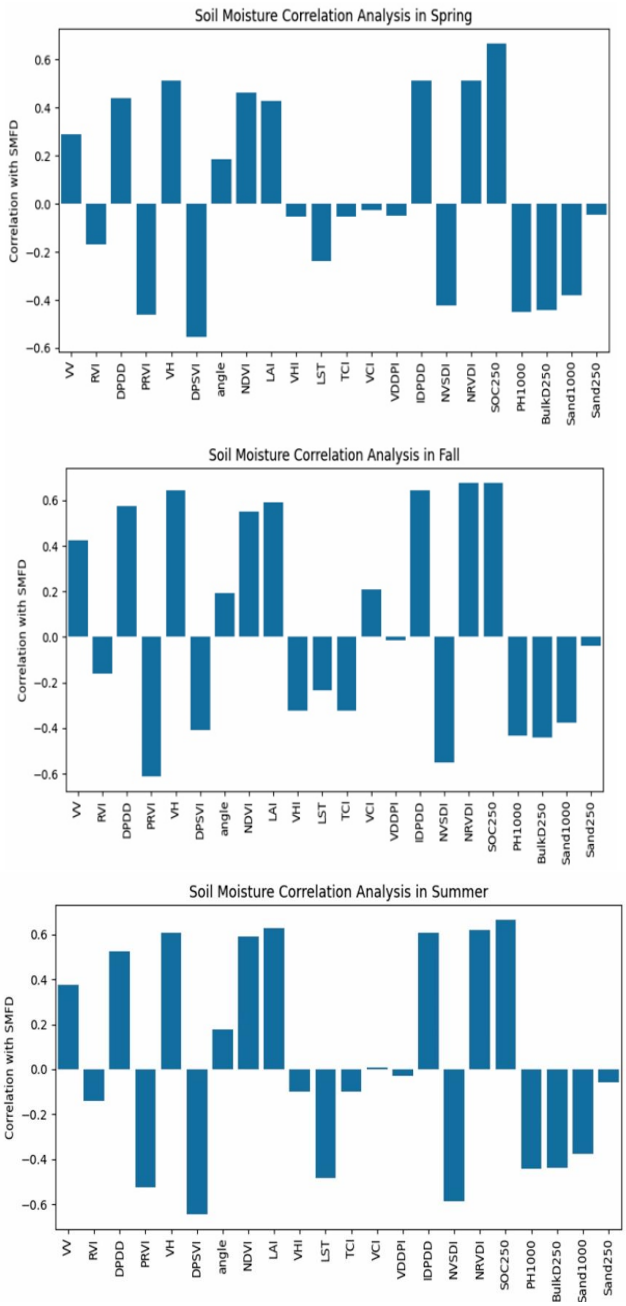

Figure 5. bar chart between parameters and the Soil Moisture Fusion Dataset (SMFD) in different seasons

Figure 6 shows the importance matrix of model features for predicting soil moisture in four seasons with R^2 values. This heat map shows which features had the highest explanatory power in each season. In most seasons, the radar indices (VV, VH, DPDD), vegetation indices (NDVI, LAI, PRVI), and the soil-like property SOC250 (soil organic carbon at a depth of 250 cm) showed high explanatory power in most seasons in estimating soil moisture. In winter, predictive capability was moderate, with SOC250 achieving the highest R^2 (0.45), while radar and vegetation indices showed lower contributions, suggesting the influence of additional environmental factors. Vegetation light indices, including NDVI, NRVDI, NVSDI, and DPSVI, are especially important in summer and autumn (R^2 values up to about 0.4),

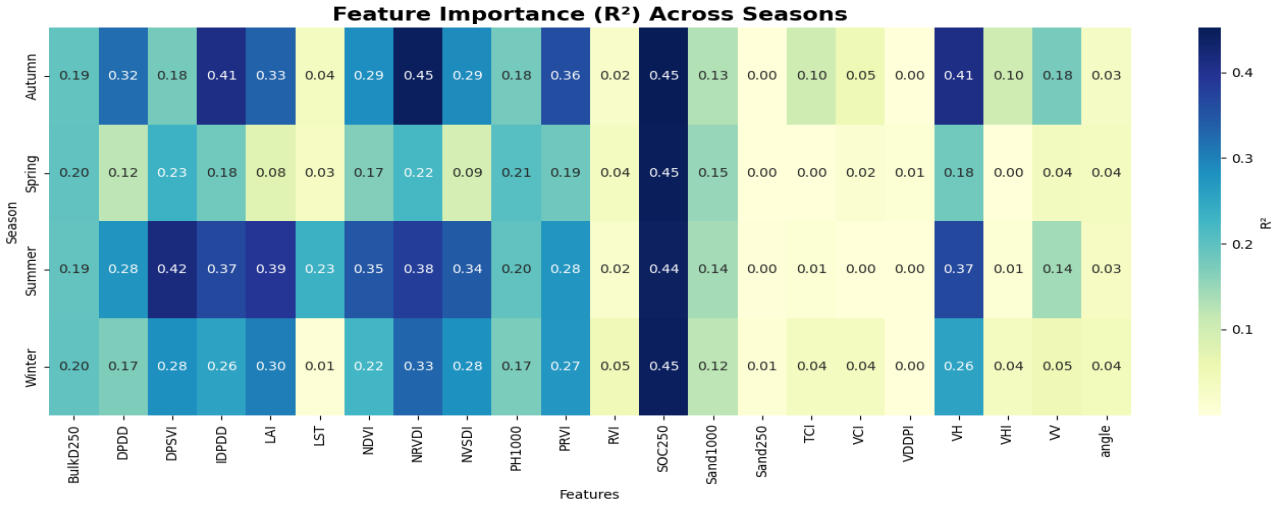

Figure 6. Seasonal Heatmap of Explanatory Power (R^2) of features used for Soil Moisture

which indicates that vegetation cover and photosynthetic activity are important factors in determining soil moisture in these seasons. The land surface temperature index (LST) is particularly influential in the summer, with an R2 of about 0.23, which indicates the role of temperature in the process of evaporation and moisture transport. Radar indices (VH, VHI) are less important in the model; however, VH is slightly more effective in autumn and winter, which is probably related to the sensitivity of the radar to surface moisture. Indices such as TCI, VCI, VDDPI, and angle are the least important and have less impact on the prediction model. The strong applicability of SOC250 and NDVI highlights their value as crucial variables guiding soil moisture contents. The difference in the importance of these indices during seasons is consistent with natural variations recorded during vegetation and soil cover seasons. This analysis provides a deeper understanding of climatic dynamics and their consequences for environmental and agricultural activities, and is useful for deriving further accurate models for controlling water and soil resources.

In this section, the importance of features is examined based on the model performance. Of the 22 features used for each season and the entire dataset (Table 3), the results of the feature ranking which is measured based on the impact of the features on the accuracy of the model. RF model showed that revealing distinct seasonal patterns where SOC250 exhibited the highest importance in winter (0.4815) and spring (0.4803), emphasizing the critical role of soil organic carbon during these periods, while in summer and fall, NDVI emerged as the dominant predictor (0.4256 and 0.2528, respectively), reflecting the influence of vegetation dynamics during active growth seasons. In the analysis of the importance of features in the SVR model for predicting soil moisture in the fall, the LAI index, with values of (0.41, 0.134, and 0.091), had high significance, respectively. Unlike spring, where soil properties were the main factor, in autumn, plant characteristics have a dominant contribution (more than 40%) in predicting soil moisture, which indicates a change in the seasonal pattern of soil and plant characteristics. Along with indices such as NVSDI, DPSVI, and NRVDI, they also showed significant contributions throughout the seasons, and based on the feature ranking, soil-related variables (Sand250, Sand1000, and BulkD250) and NDVI, NVSDI, DPSVI, NRVDI, and LAI appeared regularly in different seasons. Other features appeared intermittently. These results emphasize the necessity of integrating both soil properties and vegetation indices when modeling soil moisture, as their relative influences shift with seasonal changes (Figure 7).

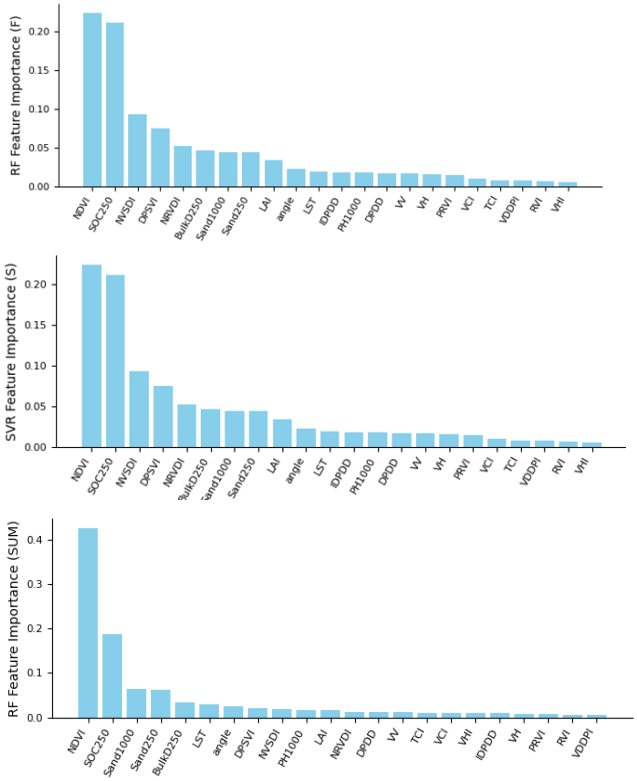

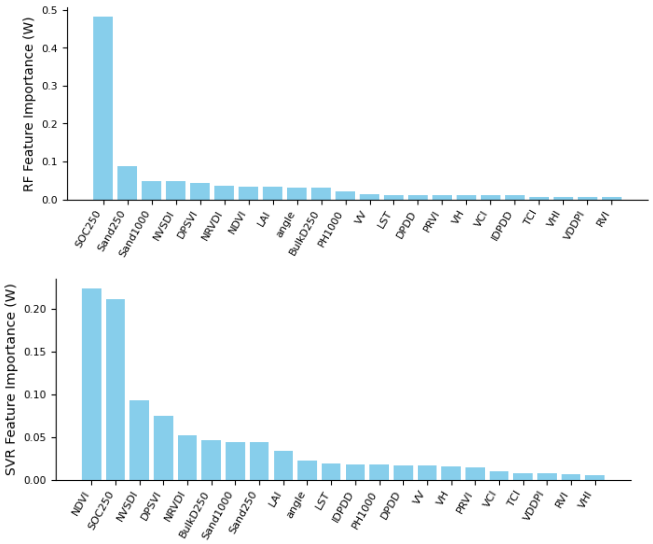

Figure 7. Bar Chart of Feature Importance Scores from Result Rf and SVR Models

The error rate in the SVR model was higher than that of the RF in all evaluation criteria, including the mean MSE, R^2, and MAE for both model runs. The SVR model has a significantly higher error rate and lower explanatory power. MAE values consistently higher than the RF model, ranging between 0.0552 and 0.0627. Notably, the RF model achieved its highest prediction performance when using the top 10 relevant features. the lowest MSE values were observed in RF of 0.0012 in winter and 0.0010 in spring. The SVR model had the lowest accuracy in summer (50.539%) and the highest accuracy (0.628%) in fall. increasing the accuracy R^2 in two runs was observed in the RF model by 0.1 to 0.3, with the highest increase in accuracy in the summer (0.80 to 0.83). The results of this study prove that the RF model, leveraging selected important features, proves to be a more robust and accurate tool for seasonal soil moisture forecasting.

Table 4. Accuracy of the random RF and SVR models in predicting soil moisture

Seasons		Used Features	Mean Squared Error	R-squared	Mean Absolute Error
Winter (w)	RF	22 F	0.0022	0.861	0.032
		10 IF	0.0012	0.87	0.022
	SVR	22 F	0.0043	0.60	0.056
		10 IF	0.0042	0.610	0.0552
Spring (S)	RF	22 F	0.0012	0.88	0.022
		10 IF	0.0010	0.90	0.019
	SVR	22 F	0.0045	0.599	0.058
		10 IF	0.0044	0.609	0.0571
Summer (SUM)	RF	22 F	0.0020	0.80	0.029
		10 IF	0.0017	0.831	0.025
	SVR	22 F	0.0048	0.539	0.06
		10 IF	0.0627	0.527	0.0627
Fall (F)	RF	22 F	0.0020	0.833	0.028
		10 IF	0.0018	0.846	0.027
	SVR	22 F	0.0045	0.6285	0.0569
		10 IF	0.0044	0.6366	0.0561

In this study, the Sensitivity analysis[81] of NRVDI and DPSVI were analyzed to evaluate the development indicators, and a mixed analytical framework, including correlation and regression components, was used to evaluate the performance of these indicators. Our comprehensive regression analysis across four seasons revealed distinct patterns in the predictive performance of vegetation cover and soil moisture indices for NDVI estimation.NVSDI and LAI indices, with mean R^2 values of 0.790 and 0.775, respectively, showed excellent predictive capabilities, making them the most reliable indicators of seasonal variation. They also appeared in the accuracy range of 0.87 to 0.93 during winter and autumn, respectively. SMFD showed a significant positive relationship with vegetation cover in all seasons and explained an average of 26.1% of the NDVI variation. The consistently high performance of NVSDI indicates that it effectively captures the biophysical properties of vegetation related to soil moisture. This relationship was particularly pronounced in the summer months (R^2 = 0.349), indicating an increased hydrological influence on vegetation dynamics during warmer periods. Relatively lower values than NVSDI and LAI, but with a high standard deviation (0.244 ± 0.122) indicate that NRVDI has relatively lower values but usually performs better in some specific seasons and can indicate that NRVDI can provide useful supplementary information, especially when other vegetation indices do not show changes well.

Table 5. Sensitivity analysis and seasonal performance of NRVDI and DPSVI indices in NDVI prediction

Index	NVSDI	LAI	SMFD	NRVDI	PRVI
Winter	0.871	0.861	0.225	0.25	0.262
Spring	0.436	0.382	0.166	0.056	0.061
Summer	0.924	0.921	0.349	0.343	0.298
Fall	0.928	0.937	0.304	0.325	0.297
Mean a± SD	0.790 a ± .0228	.0775 a ± .0252	.0261 a.0 ±077	.0244 a.0 ±122	.0230 a.0 ±108

Here are some examples of regression plots used in sensitivity analysis to examine explanatory power. The results show that NVSDI has a very strong negative linear relationship with NDVI during both summer and fall seasons, with coefficients of determination R2 of 0.924 and 0.928, respectively. This indicates that as NVSDI increases, NDVI decreases in a tightly coupled manner, suggesting that NVSDI effectively captures structural changes in vegetation linked to leaf area and scattering properties. In contrast, NRVDI demonstrates a moderate positive correlation with NDVI (summer = 0.325). This suggests that while NRVDI reflects some vegetation variations detectable by radar backscatter differences, it also has a more accurate relative DPSVI and PAR alone. These findings suggest that NVSDI, integrating structural scattering information (DPSVI) and canopy properties

(LAI), provides a more reliable indicator of vegetation changes in relation to NDVI than NRVDI, which relies on radar vegetation difference ratios. This makes NVSDI a stronger candidate for inclusion in multi-sensor remote sensing models aiming to estimate vegetation health or soil moisture dynamics based on combined optical-radar indices.

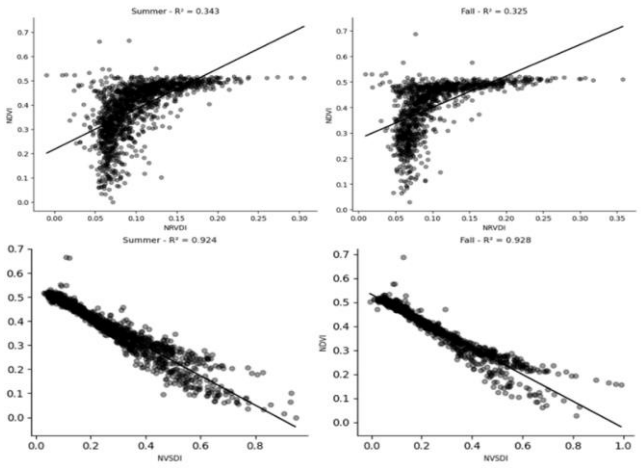

Figure 8. Sensitivity analysis regression NVSDI and NRVDI indicators vs NDVI

The prediction performance of the soil moisture estimation model was assessed through statistical comparisons between observed and predicted soil moisture values for 12 and 30 October using linear regression (Figure9), which for 12 and 30 October, respectively, showed R2 = 0.5276 and R2 = 0.35, indicating moderate correlation, meaning that approximately 52.76% of the variability in predicted moisture can be explained by the observed data. The value of R2 = 0.35, while indicating lower explanatory power, is still the average for the model at that time step, and, given the inherent variability of soil moisture and the sparse field data used, the model still shows a reasonable level of performance.

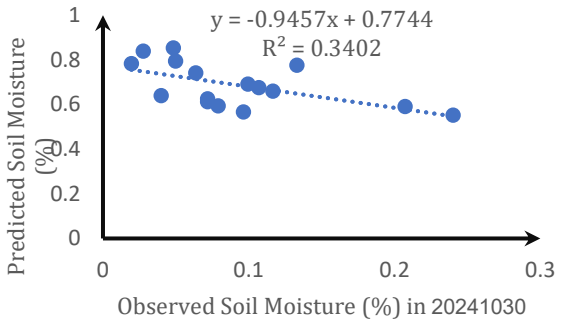

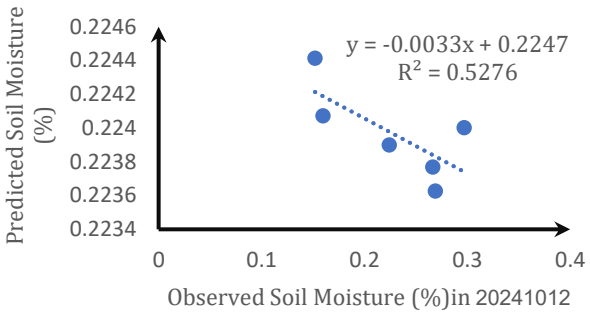

Figure 9. Comparison of observed and predicted soil moisture values with regression analysis (R^2 Value).

This reflects the difficulty of predicting dynamic environmental variables with scarce ground reality. Note that the mean R2 reflects the inherent difficulties in modeling dynamic soil moisture, influenced by the heterogeneity of the area, variability with time, limitations in the sensors, and environmental factors like rainfall and vegetative growth. Such causes of uncertainty are reflected in the variance of predictions with respect to ground reality. Despite all these challenges, the present model demonstrates great potential in connecting satellite remote sensing retrievals with actual soil moisture status. The model's performance is in fair agreement with comparable research employing machine learning algorithms and multi-sensor data fusion, reflecting improved prediction accuracy with continued refinements and the utilization of independent validation data.

4. 2. Discussion

This study is the first to integrate the effectiveness of a scalable multi-sensor framework with an emphasis on Sentinel-1 imagery in combination with a comprehensive dataset (detailed in Section 2.1)in the Urmia Lake basin, enabling high-resolution soil moisture mapping by analyzing seasonal feature priorities using two RF and SVR models. It also evaluated moisture stress indices, including for estimating seasonal moisture. Among them, LST, VHI, and VCI were of great importance in the estimation, especially in summer. It is worth noting that two combined, multispectral and radar NRDVI and NVDSI indices were proposed in this study, which complement the vegetation survey with higher efficiency than single indices, more information of which is provided in Table 2. Our seasonal analysis revealed dynamic changes in feature 6 across different seasons. This finding is consistent with the work of Shahriyari et al, who found that indices derived from Sentinel-1 images were significant in winter, likely due to the impact of plant water content on radar backscatter. In contrast, vegetation indices like NDVI, LAI, and NVDSI were the primary influencers in summer and Fall, as well as Menon and Lim [79] and Huang et al. [82], who reported the correlation between SOC and soil moisture. The importance of DPSVI and NRDVI in colder seasons was confirmed by Mandal et al. [83] and Luca et al. [84], emphasizing the variable nature of vegetation and environmental conditions during autumn, winter, and spring. NVDSI and NDVI were notable features following radar indices during these seasons. The local irradiation

angle (LIA) remained consistently important throughout all seasons, aligning with the studies of Shahriari et al. [82]. Additionally, Nativea et al. [14], discussed vegetation-mediated effects on radar backscatter, supporting these observations. Together, these results highlight the complex interactions among seasonal vegetation dynamics, climate, and soil properties. The comparison of RF and SVR algorithms underscores significant strengths. findings from Dai et al. [85], Hussain et al. [86], and Chen et al. [87] RF using Sentinel-1 data and different datasets had good robustness and sensitivity to soil moisture changes and anomalies during seasonal transitions. Pasolli et al. [45] also noted that SVR is inherently robust to noise in the training data, which can contribute to its robustness under diverse environmental conditions. Native et al. [54] discussed vegetation-mediated effects on radar backscatter. Collectively, these patterns underscore the complex interplay between seasonal vegetation dynamics, climatic conditions, and soil properties.

Although our study evaluated seasonal performance, a more rigorous quantification of model uncertainty and an assessment of spatial transferability to other regions are necessary to fully establish the model's robustness and general applicability [67, 88]. Despite the strong performance, several limitations must be acknowledged. First, the vegetation penetration limitations of C-band SAR sensors may restrict accuracy in densely vegetated areas. Second, the reliance on the FLDAS soil moisture product, with its relatively coarse spatial resolution (1-9 km), introduces inherent scale-related uncertainties (Khorrami et al, [45]. Third, the use of static soil parameters may not fully capture dynamic land-surface processes. Furthermore, remotely sensed soil moisture products can have errors in temporal continuity and spatial spread, especially when data from different seasons representing extreme soil moisture conditions are used (Koley & Jeganathan, 2019). Furthermore, the lack of field data was one of the challenges of this study, which was partially compensated for by integrating Sentinel-1 data and detailed soil characteristics. This comprehensive dataset provides a more comprehensive assessment of model limitations, strengthens the scientific rigor of our study, and suggests broader areas for future studies. Future research should pursue two promising directions. First, integrating the dataset from this study with observations from SMAP and SMOS missions would enable a more comprehensive validation across different spatial scales and improve the generalization of findings across diverse environmental conditions. Second, developing hybrid modeling approaches that combine physical models (such as the Water Cloud Model) with machine learning architectures could leverage the strengths of both methods. These hybrid models should specifically incorporate feature priority analysis, considering the seasonal variability in the importance of vegetation indices, soil properties, and radar parameters to enhance both accuracy and adaptability across different seasons and geographical areas.

5. Conclusions

This study developed a seasonal surface soil moisture estimation framework for Lake Urmia Basin by integrating multi-sensor satellite data (Sentinel-1, Sentinel-2, Landsat-8) with SoilGrids and FLDAS datasets. Two machine learning algorithms (RF and SVR) were evaluated using 22 features derived from 5386 samples collected between 2020-2024Initial seasonal correlation analysis revealed strong relationships among most variables, with correlation patterns between environmental factors and soil moisture demonstrating complex seasonal dynamics. Land Surface Temperature (LST) emerged as a particularly important feature during summer. Feature importance analysis identified soil organic carbon (SOC), sand content, NDVI, LAI, DPSVI, and radar backscatter (VH, VV) as consistently influential predictors across seasons. Initial seasonal correlation analysis revealed strong relationships among most variables, with correlation patterns between environmental factors and soil moisture demonstrating complex seasonal dynamics. Land Surface Temperature (LST) emerged as a particularly important feature during summer. Feature importance analysis identified soil organic carbon (SOC), sand content, NDVI, LAI, DPSVI, and radar backscatter (VH/VV) as consistently influential predictors across seasons.

Analysis revealed a strong negative relationship between DPSVI and vegetation indices (LAI/NDVI), where higher DPSVI values indicated reduced vegetation growth. The NVSDI and LAI indices proved to be reliable predictors of seasonal vegetation dynamics, effectively reflecting soil moisture conditions. The inclusion of NRVDI as a complementary index enhanced model performance by capturing more vegetation-soil moisture interactions, especially in specific seasonal conditions where other indices may perform poorly. These findings underscore the importance of considering seasonal variability and multiple environmental factors to accurately model and predict soil moisture dynamics. Using feature selection and reducing the model to the most influential variables improved predictive accuracy, in summer, showing a 1.2% increase in R^2 when using the selected feature subset compared to all variables. Also, the accuracy evaluation results of the model for October 12 and 30 indicate a moderate correlation between the predicted data and field observations with R^2 values of 0.5276 and 0.35, respectively. Soil organic carbon (SOC) enhances soil water retention during colder months by improving soil structure and reducing evaporation when plant transpiration is low, as Menon and Lim[79]expressed book. Conversely, NDVI and LAI vegetation indices prevailed in summer and Fall, reflecting active vegetation regulating soil moisture through transpiration, consistent with patterns observed in global agroecosystem studies, reflecting active vegetation regulating soil moisture through transpiration, a pattern also observed by Shahriari et al. [36] and Li et al. [40] This dimensionality reduction enhances computational efficiency and model interpretability without sacrificing performance. This study achieved a significant advancement in high-resolution soil moisture estimation through an innovative multi-sensor data integration framework. New composite

indices (NRDVI and NVDSI) were developed to better capture vegetation-soil moisture interactions. A pioneering seasonal feature priority analysis revealed complex dynamics of influencing factors across different seasons, resulting in highly accurate and interpretable machine learning models (particularly RF) that demonstrated high accuracy (R^2 = 0.90) at the basin scale. Collectively, these findings provide a solid foundation for enhancing water and soil resource management, particularly in agricultural zones prone to climatic constraints.

Acknowledgment

The authors express their gratitude to the European Space Agency (ESA) for the freely available Sentinel-1 and multispectral data, which were crucial for this study.

Author contributions

Maryam Sadeghi: SAR and multispectral data processing, fieldwork, data curation, visualization, original draft preparation. Khalil Valizadeh Kamran: Project administration, conceptualization, methodology design, supervision, review, and editing of the manuscript. Sadra Karimzadeh: methodological framework development, SAR data analysis, visualization, and contribution to writing the original draft. Abolfazl Ghanbari: supervision, statistical analysis, assistance in data interpretation, and review of results. Saeed Samadian Fard: conceptualization, methodological framework development, supervision, technical validation, programming, and editing of the manuscript.

Conflicts of interest

The authors declare no conflicts of interest.

References

1. Ma, C., Li, X., & McCabe, M. F. (2020). Retrieval of high-resolution soil moisture through a combination of Sentinel-1 and Sentinel-2 data. Remote Sensing, 12(14), 1–28. https://doi.org/10.3390/rs12142303
2. Çelik, M. Ö., Kuşak, L., & Yakar, M. (2024). Assessment of groundwater potential zones utilizing geographic information system-based analytical hierarchy process, Vlse Kriterijumska Optimizacija Kompromisno Resenje, and technique for order preference by similarity to ideal solution methods: a case study in Mersin, Türkiye. Sustainability, 16(5), 2202.
3. Rabhi, L., Falih, N., Afraites, L., & Bouikhalene, B. (2021). Digital agriculture based on big data analytics: A focus on predictive irrigation for smart farming in Morocco. Indonesian Journal of Electrical Engineering and Computer Science, 24(1), 581–589. https://doi.org/10.11591/ijeecs.v24.i1.pp581-589
4. Veloso, A., Mermoz, S., Bouvet, A., Le Toan, T., Planells, M., Dejoux, J. F., & Ceschia, E. (2017). Understanding the temporal behavior of crops using Sentinel-1 and Sentinel-2-like data for agricultural applications. Remote Sensing of Environment, 199, 415–426. https://doi.org/10.1016/j.rse.2017.07.015
5. Tronquo, E., Lievens, H., Bouchat, J., Defourny, P., Baghdadi, N., & Verhoest, N. E. C. (2022). Soil Moisture Retrieval Using Multistatic L-Band SAR and Effective Roughness Modeling. Remote Sensing, 14(7), 1–23. https://doi.org/10.3390/rs14071650
6. Cha, Y., Park, S. S., Kim, K., Byeon, M., & Stow, C. A. (2014). Water Resources Research, 5375–5377. https://doi.org/10.1002/2013WR014979.Reply
7. Mohanty, B. P., Cosh, M. H., Lakshmi, V., & Montzka, C. (2017). Soil Moisture Remote Sensing: State-of-the-Science. Vadose Zone Journal, 16(1), 1–9. https://doi.org/10.2136/vzj2016.10.0105
8. Unel, F. B., Kusak, L., Yakar, M., Sahin, A., Dogan, H., & Demir, F. (2025). Statistical and Visual Evaluation of Artificial Neural Networks and Multiple Linear Regression Performances in Estimating Reference Crop Evapotranspiration for Mersin. Revue Internationale de Geomatique, 34(1), 433-460.
9. Sabaghy, S., Walker, J. P., Renzullo, L. J., & Jackson, T. J. (2018). Spatially enhanced passive microwave-derived soil moisture: Capabilities and opportunities. Remote Sensing of Environment, 209(January), 551–580. https://doi.org/10.1016/j.rse.2018.02.065
10. Ezzahar, J., Ouaadi, N., Zribi, M., Elfarkh, J., Aouade, G., Khabba, S., … Jarlan, L. (2020). Evaluation of backscattering models and support vector machine for the retrieval of bare soil moisture from Sentinel-1 data. Remote Sensing, 12(1), 1–20. https://doi.org/10.3390/RS12010072
11. Grillakis, M. G., Koutroulis, A. G., Alexakis, D. D., Polykretis, C., & Daliakopoulos, I. N. (2021). Regionalizing Root-Zone Soil Moisture Estimates From ESA CCI Soil Water Index Using Machine Learning and Information on Soil, Vegetation, and Climate. Water Resources Research, 57(5), 1–22. https://doi.org/10.1029/2020WR029249
12. Do, S. K., Akhtar, F., Goffin, B., Aryal, A., Tran, T. N. D., Lipscomb, M., & Lakshmi, V. (2024). Assessing terrestrial water storage variations in Afghanistan using GRACE and FLDAS-Central Asia data. Journal of Hydrology: Regional Studies, 55. https://doi.org/10.1016/j.ejrh.2024.101906
13. Duysak, H., & Yigit, E. (2022). Investigation of the performance of different wavelet-based fusions of SAR and optical images using Sentinel-1 and Sentinel-2 datasets. International Journal of Engineering and Geosciences, 7(1), 81–90. https://doi.org/10.26833/ijeg.882589
14. Nativel, S., Ayari, E., Rodriguez-Fernandez, N., Baghdadi, N., Madelon, R., Albergel, C., & Zribi, M. (2022). Hybrid Methodology Using Sentinel-

1/Sentinel-2 for Soil Moisture Estimation. Remote Sensing, 14(10), 1–16. https://doi.org/10.3390/rs14102434
15. Çevikalp, M. R., Işık, M. S., Çelik, M. F., & Musaoğlu, N. (2024). CYGNSS toprak nemi verilerinin SMAP uydusu ve ISMN istasyonları ile karşılaştırmalı analizi. Geomatik, 9(2), 227–237. https://doi.org/10.29128/geomatik.1424069
16. Atun, R., & Gursoy, O. (2024). Determining soil moisture with Sentinel-1 image. Journal of Geodesy and Geoinformation, 11(2), 149–156. https://doi.org/10.9733/jgg.2024r0010.e
17. Entekhabi, D., Njoku, E. G., O'Neill, P. E., Kellogg, K. H., Crow, W. T., Edelstein, W. N., … Van Zyl, J. (2010). The soil moisture active passive (SMAP) mission. Proceedings of the IEEE, 98(5), 704–716. https://doi.org/10.1109/JPROC.2010.2043918
18. Notarnicola, C., Angiulli, M., & Posa, F. (2006). Use of radar and optical remotely sensed data for soil moisture retrieval over vegetated areas. IEEE Transactions on Geoscience and Remote Sensing, 44(4), 925–934. https://doi.org/10.1109/TGRS.2006.872287
19. Baghdadi, N., Hajj, M. El, Zribi, M., & Bousbih, S. (2017). Calibration of the Water Cloud Model at C-Band for winter crop fields and grasslands. Remote Sensing, 9(9), 1–13. https://doi.org/10.3390/rs9090969
20. Desai, G. T., & Gaikwad, A. N. (2024). Soil moisture estimation using ground scatterometer and Sentinel-1 data. Bulletin of Electrical Engineering and Informatics, 13(3), 1707–1717. https://doi.org/10.11591/eei.v13i3.6433
21. Mansoor, A., & Shahzad, L. (2025). Climate Change in Agriculture: Impacts, Adaptation, and Mitigation. https://doi.org/10.1007/978-981-96-2413-3_13
22. Aggarwal, P. K., & Singh, S. D. (n.d.). Climate Change Impact , Adaptation and Mitigation in Agriculture : Editors. https://ccafs.cgiar.org
23. Mandal, D., Kumar, V., Ratha, D., Dey, S., Bhattacharya, A., Lopez-Sanchez, J. M., … Rao, Y. S. (2020). Dual polarimetric radar vegetation index for crop growth monitoring using sentinel-1 SAR data. Remote Sensing of Environment, 247. https://doi.org/10.1016/j.rse.2020.111954
24. He, B., Xing, M., & Bai, X. (2014). A synergistic methodology for soil moisture estimation in an alpine prairie using radar and optical satellite data. Remote Sensing, 6(11), 10966–10985. https://doi.org/10.3390/rs61110966
25. Yilmaz, V. (2025). Climate patterns in Europe: A focus on ten countries through remote sensing. International Journal of Engineering and Geosciences, 10(3), 398–418. https://doi.org/10.26833/ijeg.1583206
26. Mogaraju, J. K. (2024). Machine learning assisted prediction of land surface temperature (LST) based on major air pollutants over the Annamayya District of India. International Journal of Engineering and Geosciences, 9(2), 233–246. https://doi.org/10.26833/ijeg.1394111
27. Uyar, N. (2024). Effects of Climate Change and Air Pollution on Soil Moisture : The Case of Türkiye İklim Değişikliği ve Hava Kirliliğinin Toprak Nemi Üzerindeki Etkileri : Türkiye Örneği, 3(2), 135–152.
28. Ghasemian Sorboni, N., Pahlavani, P., & Bigdeli, B. (2019). Vegetation mapping of sentinel-1 and 2 satellite images using convolutional neural network and random forest with the aid of dual-polarized and optical vegetation indexes. In International Archives of the Photogrammetry, Remote Sensing and Spatial Information Sciences - ISPRS Archives (Vol. 42, pp. 435–440). International Society for Photogrammetry and Remote Sensing. https://doi.org/10.5194/isprs-archives-XLII-4-W18-435-2019
29. Bao, Y., Lin, L., Wu, S., Kwal Deng, K. A., & Petropoulos, G. P. (2018). Surface soil moisture retrievals over partially vegetated areas from the synergy of Sentinel-1 and Landsat 8 data using a modified water-cloud model. International Journal of Applied Earth Observation and Geoinformation, 72(March), 76–85. https://doi.org/10.1016/j.jag.2018.05.026
30. Kseneman, M., Gleich, D., & Čučej, Ž. (2011). Soil moisture estimation using high-resolution spotlight terraSAR-X data. IEEE Geoscience and Remote Sensing Letters, 8(4), 686–690. https://doi.org/10.1109/LGRS.2010.2099641
31. Mallah, S., Delsouz Khaki, B., Davatgar, N., Scholten, T., Amirian-Chakan, A., Emadi, M., … Taghizadeh-Mehrjardi, R. (2022). Predicting Soil Textural Classes Using Random Forest Models: Learning from Imbalanced Dataset. Agronomy, 12(11), 1–16. https://doi.org/10.3390/agronomy12112613
32. Jia, Y., Jin, S., Savi, P., Yan, Q., & Li, W. (2020). Modeling and theoretical analysis of gnss-r soil moisture retrieval based on the random forest and support vector machine learning approach. Remote Sensing, 12(22), 1–24. https://doi.org/10.3390/rs12223679
33. Pokhariyal, S., Patel, N. R., & Govind, A. (2023). Machine Learning-Driven Remote Sensing Applications for Agriculture in India—A Systematic Review. Agronomy, 13(9), 1–30. https://doi.org/10.3390/agronomy13092302
34. Uddin, S., Khan, A., Hossain, M. E., & Moni, M. A. (2019). Comparing different supervised machine learning algorithms for disease prediction. BMC Medical Informatics and Decision Making, 19(1), 1–16. https://doi.org/10.1186/s12911-019-1004-8
35. Vollrath, A., Mullissa, A., & Reiche, J. (2020). Angular-based radiometric slope correction for

Sentinel-1 on google earth engine. Remote Sensing, 12(11), 1–14. https://doi.org/10.3390/rs12111867

36. Shahriari, M. A., Aghighi, H., Azadbakht, M., Ashourloo, D., Matkan, A. A., Brakhasi, F., & Walker, J. P. (2025). Soil moisture estimation using combined SAR and optical imagery: Application of seasonal machine learning algorithms. Advances in Space Research, (xxxx). https://doi.org/10.1016/j.asr.2025.01.064
37. Li, A., Tan, X., Wu, W., Liu, H., & Zhu, J. (2017). Predicting active-layer soil thickness using topographic variables at a small watershed scale. PLoS ONE, 12(9), 1–17. https://doi.org/10.1371/journal.pone.0183742
38. Géant, C. B., Gustave, M. N., & Schmitz, S. (2023). Mapping small inland wetlands in the South-Kivu province by integrating optical and SAR data with statistical models for accurate distribution assessment. Scientific Reports, 13(1), 1–23. https://doi.org/10.1038/s41598-023-43292-7
39. Shahriari, M. A., Aghighi, H., Azadbakht, M., Ashourloo, D., Matkan, A. A., Brakhasi, F., & Walker, J. P. (2025). Soil moisture estimation using combined SAR and optical imagery: Application of seasonal machine learning algorithms. Advances in Space Research, 75(8), 6207–6221. https://doi.org/10.1016/j.asr.2025.01.064
40. Li, W., Migliavacca, M., Forkel, M., Denissen, J. M. C., Reichstein, M., Yang, H., … Orth, R. (2022). Widespread increasing vegetation sensitivity to soil moisture. Nature Communications, 13(1), 1–9. https://doi.org/10.1038/s41467-022-31667-9
41. Barh, D., Khan, M. S., & Davies, E. (2015). PlantOmics: The omics of plant science. PlantOmics: The Omics of Plant Science. https://doi.org/10.1007/978-81-322-2172-2
42. Lamichhane, M., Mehan, S., & Mankin, K. R. (2025). Soil Moisture Prediction Using Remote Sensing and Machine Learning Algorithms: A Review on Progress, Challenges, and Opportunities. Remote Sensing, 17(14). https://doi.org/10.3390/rs17142397
43. Liu, S., Wang, X., Liu, M., & Zhu, J. (2017). Towards better analysis of machine learning models: A visual analytics perspective. Visual Informatics, 1(1), 48–56. https://doi.org/10.1016/j.visinf.2017.01.006
44. Feizizadeh, B., Yariyan, P., Yakar, M., Blaschke, T., & Almuraqab, N. A. S. (2025). An integrated hybrid deep learning data driven approaches for spatiotemporal mapping of land susceptibility to salt/dust emissions. Advances in Space Research.
45. Vahidi, M., Shafian, S., & Frame, W. H. (2025). Precision Soil Moisture Monitoring Through Drone-Based Hyperspectral Imaging and PCA-Driven Machine Learning. Sensors, 25(3). https://doi.org/10.3390/s25030782
46. Asadollah, S. B. H. S., Sharafati, A., Saeedi, M., & Shahid, S. (2024). Estimation of soil moisture from remote sensing products using an ensemble machine learning model: a case study of Lake Urmia Basin, Iran. Earth Science Informatics, 17(1), 385–400. https://doi.org/10.1007/s12145-023-01172-8
47. Feizizadeh, B., Abdollahi, Z., & Shokati, B. (2022). A GIS-Based Spatiotemporal Impact Assessment of Droughts in the Hyper-Saline Urmia Lake Basin on the Hydro-Geochemical Quality of Nearby Aquifers. Remote Sensing, 14(11). https://doi.org/10.3390/rs14112516
48. Soltani, K., & Azari, A. (2024). Terrestrial water storage anomaly estimating using machine learning techniques and satellite-based data (a case study of Lake Urmia Basin). Irrigation and Drainage, 73(1), 215–229. https://doi.org/10.1002/ird.2863
49. Hesami, A., & Amini, A. (2016). Changes in irrigated land and agricultural water use in the Lake Urmia basin. Lake and Reservoir Management, 32(3), 288–296. https://doi.org/10.1080/10402381.2016.1211202
50. Hengl, T., De Jesus, J. M., MacMillan, R. A., Batjes, N. H., Heuvelink, G. B. M., Ribeiro, E., … Gonzalez, M. R. (2014). SoilGrids1km - Global soil information based on automated mapping. PLoS ONE, 9(8). https://doi.org/10.1371/journal.pone.0105992
51. Radočaj, D., Jurišić, M., Rapčan, I., Domazetović, F., Milošević, R., & Plaščak, I. (2023). An Independent Validation of SoilGrids Accuracy for Soil Texture Components in Croatia. Land, 12(5). https://doi.org/10.3390/land12051034
52. Schubert, A. (2022). Guide to S-1 Geocoding Guide to Sentinel-1 Geocoding. https://sentiwiki.copernicus.eu
53. Sorokin, A., Stepanov, A., Dubrovin, K., & Verkhoturov, A. (2024). Enhancement of Comparative Assessment Approaches for Synthetic Aperture Radar (SAR) Vegetation Indices for Crop Monitoring and Identification—Khabarovsk Territory (Russia) Case Study. Remote Sensing, 16(14). https://doi.org/10.3390/rs16142532
54. de Roos, S., Bechtold, M., Busschaert, L., Lievens, H., & De Lannoy, G. J. M. (2024). Assimilation of Sentinel-1 Backscatter to Update AquaCrop Estimates of Soil Moisture and Crop Biomass. Journal of Geophysical Research: Biogeosciences, 129(10). https://doi.org/10.1029/2024JG008231
55. Sorokin, A., Stepanov, A., Dubrovin, K., & Verkhoturov, A. (2024). Enhancement of Comparative Assessment Approaches for Synthetic Aperture Radar (SAR) Vegetation Indices for Crop Monitoring and Identification—Khabarovsk Territory (Russia) Case Study. Remote Sensing, 16(14). https://doi.org/10.3390/rs16142532

56. Das, D. P., & Pandey, A. (2025). Soil moisture retrieval from dual-polarized Sentinel-1 SAR data over agricultural regions using a water cloud model. Environmental Monitoring and Assessment, 197(1). https://doi.org/10.1007/s10661-024-13510-4
57. Periasamy, S. (2018). Significance of dual polarimetric synthetic aperture radar in biomass retrieval: An attempt on Sentinel-1. Remote Sensing of Environment, 217(April), 537–549. https://doi.org/10.1016/j.rse.2018.09.003
58. Periasamy, S. (2018). Significance of dual polarimetric synthetic aperture radar in biomass retrieval: An attempt on Sentinel-1. Remote Sensing of Environment, 217(September), 537–549. https://doi.org/10.1016/j.rse.2018.09.003
59. Raksapatcharawong, M., Veerakachen, W., Homma, K., Maki, M., & Oki, K. (2020). Satellite-based drought impact assessment on rice yield in Thailand with SIMRIW-RS. Remote Sensing, 12(13). https://doi.org/10.3390/rs12132099
60. Santos, E. P. dos, Moreira, M. C., Fernandes-Filho, E. I., Demattê, J. A. M., Dionizio, E. A., Silva, D. D. da, … Costa, M. H. (2023). Sentinel-1 Imagery Used for Estimation of Soil Organic Carbon by Dual-Polarization SAR Vegetation Indices. Remote Sensing, 15(23). https://doi.org/10.3390/rs15235464
61. Yaman, Ş., & Tunç Görmüş, E. (2025). Sentinel-2 ve Landsat-8 ile Bulut Tabanlı Orman Yangın Analizi. Geomatik, 10(3), 316–330. https://doi.org/10.29128/geomatik.1603707
62. Şenol, H. İ., Kaya, Y., Yiğit, A. Y., & Yakar, M. (2024). Extraction and geospatial analysis of the Hersek Lagoon shoreline with Sentinel-2 satellite data. Survey Review, 56(397), 367-382.
63. Kogan, F. N. (2001). Operational space technology for global vegetation assessment. Bulletin of the American Meteorological Society, 82(9), 1949–1964. https://doi.org/10.1175/1520-0477(2001)082<1949:OSTFGV>2.3.CO;2
64. de Roos, S., Bechtold, M., Busschaert, L., Lievens, H., & De Lannoy, G. J. M. (2024). Assimilation of Sentinel-1 Backscatter to Update AquaCrop Estimates of Soil Moisture and Crop Biomass. Journal of Geophysical Research: Biogeosciences, 129(10), 1–29. https://doi.org/10.1029/2024JG008231
65. Bento, V. A., Gouveia, C. M., DaCamara, C. C., & Trigo, I. F. (2018). A climatological assessment of drought impact on vegetation health index. Agricultural and Forest Meteorology, 259(September), 286–295. https://doi.org/10.1016/j.agrformet.2018.05.014
66. Santos, E. P. dos, Santos, I. C., Bussinguer, J. de F., Cruz, R. R. P., Amaral, C. H. do, Silva, D. D. da, & Moreira, M. C. (2024). Dual-polarization vegetation indices for the Sentinel-1 sar sensor and its correlation to forest biomass from Atlantic Forest fragments. Cerne, 30(30), 1–10. https://doi.org/10.1590/01047760202330013286
67. Souissi, R., Al Bitar, A., & Zribi, M. (2020). Accuracy and transferability of artificial neural networks in predicting in situ root-zone soil moisture for various regions across the globe. Water (Switzerland), 12(11), 1–20. https://doi.org/10.3390/w12113109
68. Carrasco, L., O'Neil, A. W., Daniel Morton, R., & Rowland, C. S. (2019). Evaluating combinations of temporally aggregated Sentinel-1, Sentinel-2 and Landsat 8 for land cover mapping with Google Earth Engine. Remote Sensing, 11(3). https://doi.org/10.3390/rs11030288
69. Atun, R., Gürsoy, Ö., & Koşaroğlu, S. (2024). Field Scale Soil Moisture Estimation with Ground Penetrating Radar and Sentinel 1 Data. Sustainability (Switzerland), 16(24). https://doi.org/10.3390/su162410995
70. Mullissa, A., Vollrath, A., Odongo-Braun, C., Slagter, B., Balling, J., Gou, Y., … Reiche, J. (2021). Sentinel-1 sar backscatter analysis ready data preparation in google earth engine. Remote Sensing, 13(10), 5–11. https://doi.org/10.3390/rs13101954
71. Kadı, F., & Yılmaz, O. S. (2024). Orman içi açıklıklara ait zamansal değişimlerin uzaktan algılama teknikleri ile Google Earth Engine platformunda tespit edilmesi: Trabzon-Düzköy İlçesi örneği. Geomatik, 9(2), 141–155. https://doi.org/10.29128/geomatik.1363873
72. Ebadi, R., Karımzadeh, S., Valizadeh Kamran, K., & Mahdavifard, M. (2025). Integrating Vegetation Indices and PRISMA Hyperspectral Imagery for Forest Risk Assessment in Northern Iran. International Journal of Engineering and Geosciences, 11(1), 163–182. https://doi.org/10.26833/ijeg.1640355
73. Hird, J. N., DeLancey, E. R., McDermid, G. J., & Kariyeva, J. (2017). Google earth engine, open-access satellite data, and machine learning in support of large-area probabilisticwetland mapping. Remote Sensing, 9(12). https://doi.org/10.3390/rs9121315
74. Nofrizal, A. Y., Sonobe, R., Yamashita, H., Morita, A., & Ikka, T. (2022). Estimating chlorophyll content of Zizania latifolia with hyperspectral data and random forest. International Journal of Engineering and Geosciences, 7(3), 221–228. https://doi.org/10.26833/ijeg.953188
75. Biau, G., & Scornet, E. (2016). A random forest guided tour. Test, 25(2), 197–227. https://doi.org/10.1007/s11749-016-0481-7
76. Cai, Y., Fang, Y., Huang, F., & Fan, L. (2024). Case study on the optimal scaling factor for semantic segmentation of remote sensing image. 2024 International Conference on Machine Intelligence for GeoAnalytics and Remote Sensing, MIGARS 2024, 1–3.

https://doi.org/10.1109/MIGARS61408.2024.10544785
77. Guo, J., Bai, Q., Guo, W., Bu, Z., & Zhang, W. (2022). Soil moisture content estimation in winter wheat planting area for multi-source sensing data using CNNR. Computers and Electronics in Agriculture, 193(August 2021), 106670. https://doi.org/10.1016/j.compag.2021.106670
78. Carranza, C., Nolet, C., Pezij, M., & van der Ploeg, M. (2021). Root zone soil moisture estimation with Random Forest. Journal of Hydrology, 593(December 2020), 125840. https://doi.org/10.1016/j.jhydrol.2020.125840
79. Menon, A., & Lim, J. (2017). Hidden potential carbon. Banking. https://openknowledge.fao.org
80. Report, I. S. (2023). Summary for Policymakers of the Intergovernmental Panel on Climate Change. https://doi:10.59327/IPCC/AR6978929169164 7.001
81. Baghdadi, N., Zribi, M., Loumagne, C., Ansart, P., & Anguela, T. P. (2008). Analysis of TerraSAR-X data and their sensitivity to soil surface parameters over bare agricultural fields. Remote Sensing of Environment, 112(12), 4370–4379. https://doi.org/10.1016/j.rse.2008.08.004
82. Huang, J., Yu, H., Guan, X., Wang, G., & Guo, R. (2016). Accelerated dryland expansion under climate change. Nature Climate Change, 6(2), 166–171. https://doi.org/10.1038/nclimate2837
83. Mandal, D., Kumar, V., Ratha, D., Dey, S., Bhattacharya, A., Lopez-Sanchez, J. M., … Rao, Y. S. (2020). Dual polarimetric radar vegetation index for crop growth monitoring using Sentinel-1 SAR data. Remote Sensing of Environment, 247. https://doi.org/10.1016/j.rse.2020.111954
84. De Luca, G., Silva, J. M. N., & Modica, G. (2022). Short-term temporal and spatial analysis for post-fire vegetation regrowth characterization and mapping in a Mediterranean ecosystem using optical and SAR image time-series. Geocarto International, 37(27), 15428–15462. https://doi.org/10.1080/10106049.2022.2097482
85. Dai, J., Zhu, L., & Walker, J. (2023). Machine Learning Methods for 1 km Soil Moisture Retrieval from Sentinel-1: An Evaluation with Limited Training Samples. Proceedings of the IEEE Radar Conference, 1–5. https://doi.org/10.1109/RADAR54928.2023.10371043
86. Hussain, A., Niaz, R., Almazah, M. M. A., Al-Rezami, A. Y., Cheng, H., & Tariq, A. (2025). Utilizing Logistic Regression and Random Forest to Model Meteorological Drought Persistence Across Seasonal Transitions. Earth Systems and Environment. https://doi.org/10.1007/s41748-025-00682-3
87. Chen, P. Y., Chen, C. C., Kang, C., Liu, J. W., & Li, Y. H. (2025). Soil water content prediction across seasons using random forest based on precipitation-related data. Computers and Electronics in Agriculture, 230(September 2024), 109802. https://doi.org/10.1016/j.compag.2024.109802
88. Jiaxin, Q., Jie, Y., Weidong, S., Lingli, Z., Lei, S., & Chaoya, D. (2024). Evaluation and improvement of temporal robustness and transfer performance of surface soil moisture estimated by machine learning regression algorithms. Computers and Electronics in Agriculture, 217(January), 108518. https://doi.org/10.1016/j.compag.2023.108518